ECT-LSTM-RNN: An Electrical Capacitance Tomography Model-Based Long Short-Term Memory Recurrent Neural Networks for Conductive Materials

WAEL DEABES[1,2], **(Member, IEEE), ALAA SHETA**[3], **(Member, IEEE),**
AND MALIK BRAIK[4], **(Member, IEEE)**
[1]Department of Computer Science in Jamoum, Umm Al-Qura University, Makkah 25371, Saudi Arabia
[2]Department of Computer and Systems Engineering, Mansoura University, Mansoura 35516, Egypt
[3]Department of Computer Science, Southern Connecticut State University, New Haven, CT 06515, USA
[4]Department of Computer Science, Al-Balqa Applied University, Al-Salt 19117, Jordan

Corresponding author: Wael Deabes (wadeabes@uqu.edu.sa)

ABSTRACT Image reconstruction for industrial applications based on Electrical Capacitance Tomography (ECT) has been broadly applied. The goal of image reconstruction based ECT is to locate the distribution of permittivity for the dielectric substances along the cross-section based on the collected capacitance data. In the ECT-based image reconstruction process: (1) the relationship between capacitance measurements and permittivity distribution is nonlinear, (2) the capacitance measurements collected during image reconstruction are inadequate due to the limited number of electrodes, and (3) the reconstruction process is subject to noise leading to an ill-posed problem. Thence, constructing an accurate algorithm for real images is critical to overcoming such restrictions. This paper presents novel image reconstruction methods using Deep Learning for solving the forward and inverse problems of the ECT system for generating high-quality images of conductive materials in the Lost Foam Casting (LFC) process. Here, Long Short-Term Memory Recurrent Neural Network (LSTM-RNN) models were implemented to predict the distribution of metal filling for the LFC process-based ECT. The recurrent connection and the gating mechanism of the LSTM is capable of extracting the contextual information that is repeatedly passing through the neural network while filtering out the noise caused by adverse factors. Experimental results showed that the presented ECT-LSTM-RNN model is highly reliable for industrial applications and can be utilized for other manufacturing processes.

INDEX TERMS Image reconstruction, long short-term memory recurrent neural network, lost foam casting, metal filling process.

I. INTRODUCTION

Computed tomography is a technology to image materials distributions in closed vessels. Typically, a group of sensors is evenly mounted around the area of interest to measure one of the material properties, such as resistance, conductivity, and permittivity. Therefore, the tomography technique's selection is based on the type of material needed to be imaged. Electrical Resistive Tomography (ERT) [1], Electrical Impedance Tomography (EIT) [2], and Electrical Capacitance Tomography (ECT) [3] are well-known examples of the computed

The associate editor coordinating the review of this manuscript and approving it for publication was Frederico Guimarães.

tomography. These techniques have many advantages such as non-invasive, flexibility, fast response, low cost, and safety compared to other tomography modalities like X-Ray [4].

ECT is a well-established technique for imaging dielectric as well as conductive materials. It can induce a cross-sectional image that represents the inner distribution of conductivity based on outer capacitance measurements. ECT possesses many advantages over other tomography modalities since it is non-invasive, non-intrusive, non-radioactive, and inexpensive. It is also capable of providing detailed information about the electric properties of different flow materials [5]. Further advantages include: 1) possessing a rapid imaging speed which typically reaches 100 frames/s, 2) it does not

suffer from any hazard radiations, 3) it can bear up high temperature and high pressure. The ECT sensor is composed of multiple exciting electrodes, which are evenly mounted around the non-conductive dielectric medium of the material inside the vessel to be imaged [6]. There is an earthed screen positioned outside the electrodes to depress the exterior interference noise to accomplish such a process. The ECT system's functioning depends on gauging the change in capacitance measurement of a multi-electrode ECT sensor. This process is consummated due to the variations in the distribution and/or condensation of dielectric materials inside the vessels. The outcome is the reconstruction of cross-sectional images representing the distribution of the materials obtained from the measured data [7].

The potential applications of ECT are broadly extensive [6], with several practical and applicable domains such as biomedical [8], industrial tomography and non-destructive assessment [9]. So, there is a substantial research landscape for the successful and practical applications of ECT in a variety of target applications such as grounded metal observation in a casting process [5], imaging dilute in addition to large multi-phase flows in oil purification, in powder flow in a vertical tube for petroleum refining [10], and the food industry and observation of chemical and pharmaceutical processes [11].

There are two computational problems in the ECT system, forward and inverse problems. The **forward problem** is calculating the capacitance measurements corresponding to a known material distribution. Usually, a model of the ECT system is built using Finite Element (FE) to solve the forward problem [12]. The FEM is used to calculate a sensitivity matrix by creating a finite mesh of the imaging area, and calculating capacitance data as a linear sum of different perturbations composing different materials distributions. However, applying fixed sensitivity matrix during each iteration speeds up the inverse problem's solution, the generated images are blurred due to the linear approximation [13]. On the other hand, the **inverse problem** is generating material distribution images related to known capacitance measurements. Solutions of the inverse problem are called image reconstruction algorithms [14]. Usually, the reconstruction algorithms are ill-posed since the number of image pixels (*unknowns*) is greater than the number of capacitance measurements (*knowns*). Also, the effect of changing the material distribution on the capacitance measurements is extremely nonlinear; consequently, the inverse problem solution is a challenge task [15].

Generally, non-iterative and iterative algorithms can be used in ECT image reconstruction. However, it isn't very easy to obtain satisfactory results from the non-iterative reconstruction techniques because of the nonlinear relationship between the capacitance measurements and the materials' distribution. As a result, the iterative methods are prevalently used in the ECT to estimate the unknown distribution from the capacitance data (inverse problem) and calculate the capacitance data based on the estimated distribution to update the image in the next iteration (forward problem). A satisfactory value of the capacitance error is used to terminate the iterative loop.

A. LITERATURE REVIEW

Traditional image reconstruction algorithms such as Iterative Linear Back Projection (LBP), Landweber, iterative Tikhonov regularization, Iterative Total Variation (iTV), and Kalman Filter are still adopted; meanwhile, some distinguishing work also has been approved [3]. Adaptive Electrical Capacitance Volume Tomography (AECVT) is one instance of such a distinctive work [16]. In the AECVT, a novel ECT sensor composed of a large number of small different shapes electrodes has been developed, and accordingly, new image reconstruction algorithms dealing with such a new ECT system have been proposed [17].

The Linear Back Projection (LBP) method was presented to reconstruct an image of capacitance measurements. Initially, it fetches all electrode pairs' sensitivity distributions for an ECT system, and the normalized capacitances are then linearly superimposed using the sensitivity distributions as weighting components for obtaining images. Although the images reconstructed using the LBP method are often deformed, this algorithm remains the most widely used one due to its simplicity and rapidity. Iterative algorithms such as Landweber's iteration method [18] and algebraic reconstruction technique [19] can create significantly better images than can non-iterative reconstruction algorithms. Iterative image reconstruction methods during the practicality require long reconstruction time. So, they are only appropriate and viable for cases where rapid reconstruction time is not essential.

Currently, machine learning techniques have thrived in many fields, and many researchers have tried it to solve tomography forward and inverse problems using these techniques. A multilayer Feed-Forward Neural Network (FFNN) and analog Hopfield network have been proposed in [20] to solve both ECT problems, respectively. Boublil D. *et al.* used FFNN as a fusion image reconstruction algorithm in the computed tomography application [21]. Authors in [22] trained an Artificial Neural Network (ANN) to estimate parameters of a circular object present inside the imaging area using ECT. The obtained results showed a substantial reduction of computations time compared to the traditional iterative reconstruction image algorithms. Deabes W. *et al.* proposed Capacitance Artificial Neural Network (CANN) system in [23] as a solver for the forward problem and Metal Filled Fuzzy System (MFFS) to solve the inverse problem to construct the metal distribution images. Li *et al.* tried to generate ECT images using the Backpropagation (BP) and Radial Basis Function (RBF) neural networks [24].

Fiderek P. *et al.* applied fuzzy inference for reconstructing images of the two-phase gas-liquid flow from ECT measurement data as a sufficient alternative to the methods commonly used in the ECT field [25]. Also, Deabes W. *et al.* developed a fuzzy system to reconstruct the metal distribution profiles in the Lost Foam Casting (LFC) process [26]. In [27],

an extended sensitivity matrix consisting of some normalized capacitance vectors corresponding to the base permittivity elements is designed. Zhang L. *et al.* proposed a wavelet transform fusion algorithm to improve the quality of the ECT reconstructed images [28]. The algorithm is based on obtaining the images using conjugate gradient least square algorithm and iterative Landweber algorithm; then wavelet transform decomposes these images.

In [20], the analog Hopfield network was used to address the inverse problem based on NN with a multi-criteria optimization image reconstruction approach. This image reconstruction approach was evaluated on a set of independent capacitance measurements to reconstruct the permittivity distribution.

In recent years, Deep Learning (DL) has flourished as a robust and efficient technique in the machine learning area [29]. DL has lately been introduced to the electrical tomography field since it has a remarkable ability to map complicated nonlinear functions. Zheng J. *et al.* presented an autoencoder neural network to construct images of the ECT system [30]. Lei J. *et al.* proposed a deep learning-based inversion method to ease the reconstruction accuracy of the reconstructed ECT images [31]. Convolutions Neural Networks (CNNs) have been implemented for the EIT [32], and ERT [29]. Xiao J. *et al.* proposed two deep learning image reconstruction algorithms for electromagnetic tomography (EMT) [33]. Applying deep learning techniques to enhance and accelerate the inverse problem's solution has become crucial in ECT research. One of the novels and efficient deep learning techniques is Long Short-Term Memory Recurrent Neural Network(LSTM-RNN) [34]. LSTM-RNN can effectively generate images with detailed features depending on the provided information. Researchers in the image processing field has paid great attention to the LSTM-RNN due to its advantages [35]–[40].

Compared with convolutional and fully-connected layers, the recurrent connection and the gating mechanism of the LSTM is capable of extracting the contextual information that is repeatedly passing through the neural network while filtering out the noise caused by adverse factors. In theory, LSTM architecture can be defined to perform regression tasks by placing one output neuron without a modifying function, and that will represent a continuous output.

B. RESEARCH OBJECTIVES

This paper presents novel image reconstruction methods using DL for solving the ECT problems for generating high-quality images of conductive materials in the Lost Foam Casting (LFC) process. The main objective guiding the presented approach is to solve the reconstruction problem with a fair compromise between the goodness of the reconstructed image, robustness, and computational complexity. A better understanding of the characteristics of the molten metal inside the foam pattern is needed to reduce the fill related defects and to improve the final casting [26]. This research has two folds:
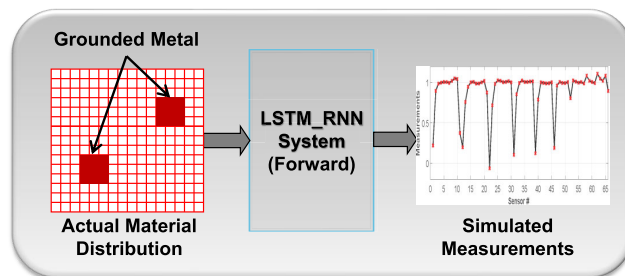

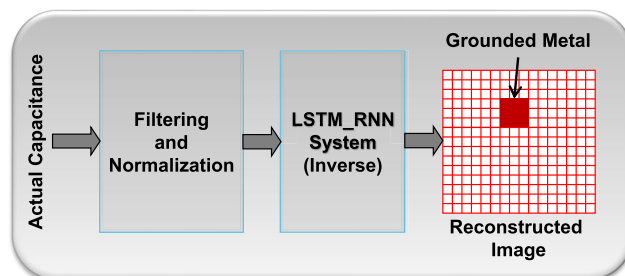**FIGURE 1.** Proposed LSTM_RNN system for forward problem.

FIGURE 2. Proposed LSTM_RNN system for inverse problem.

- A nonlinear forward solver called ECT-LSTM-RNN, shown in Fig. 1, has been developed to solve the forward problem nonlinearly with high speed and accuracy. It is based on the deep neural network (LSTM-RNN). The forward solver takes a set of known metal distributions as inputs and generates their corresponding capacitance measurements. The training data are generated based on different models developed to describe the molten metal's behavior during the casting process [41]. They are stimulated by a finite element method to calculate the capacitance measurements related to all different distributions. Some random metal distributions are generated and calculating their corresponding measurements, then used them to train the network with high accuracy.

- This work also presents a novel approach to designing a fast and accurate image reconstruction algorithm for multi-phase flow imaging during the LFC process using the LSTM-RNN [34]. The proposed ECT-LSTM-RNN inverse problem solver can create significantly high quality images than those produced by the traditional algorithms, with a lower reconstruction cost. The main objective guiding the presented approach is to solve the reconstruction problem with a fair compromise between the goodness of the reconstructed image, robustness, and computational complexity. Fig. 2 shows the proposed ECT inverse solver. Initially, the capacitance measurements C_N are pre-processed by filtering and normalization. Afterwards, the LSTM-RNN takes the measurements as inputs to produce the final reconstructed image G, which represents the metal's distribution inside the imaging area.

C. OUTLINES

This paper is organized as follows: Section II-B II presents the recent ECT system for conductive materials in the LFC
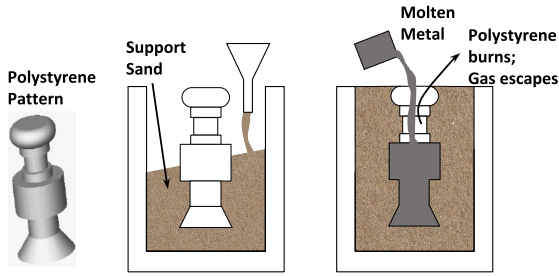
FIGURE 3. Lost Foam Casting (LFC) process.

FIGURE 4. Engine foam pattern and its final casting [42].

process. A brief look at the most common deep learning models is presented in Section III. Section IV discusses the proposed ECT-LSTM-RNN solvers for the forward and inverse problems in the ECT. Section V mainly focuses on a discussion of the simulated benchmark data sets conducted in the experiments and an explanation of the validation criteria utilized to evaluate the performance of the developed models and the results of both the forward problem and the inverse problem solvers. Finally, we present a conclusion with a broader outlook of the research direction in Section VI.

II. ECT SYSTEM FOR CONDUCTIVE MATERIALS

In the automotive industry, Lost Foam Casting (LFC) is an evaporative-pattern casting process for engine blocks [42]. LFC is a simple and inexpensive technique for casting delicately detailed, as well as complex geometries. The process goes through three steps, as shown in Fig. 3. The process starts by building a foam pattern, then supporting it inside a flask using compacted sand, and the last step is pouring the molten metal to cast the final product [43]. Fig. 4 shows an engine foam pattern and its final casting.

Monitoring how the molten metal fills the foam pattern is crucial to eliminate all related process faults and to improve the final product [44]. Typically, inferred cameras and X-Ray technology are applied to monitor the molten metal flow during the casting [45]. The X-Ray tomography suffers from hazard radiations, big size, fixed, and high cost compared to electrical tomography techniques. Therefore, many current methods have been implemented to image the industrial process [46].

The ECT is a novel feasible technology for imaging dielectric and conductive materials [47], [48]. It has high potentials,

which attract manufacturers to implement it for imaging the flow of the molten metal in the LFC process. Typically, the ECT system consists of three parts, an array of electrodes, a data acquisition unit, and a computing device [49]. For an array of $n = 12$ electrodes, shown in Fig. 5a, each pair of the electrodes makes a capacitive sensor. It is essential to optimize the ECT sensor to improve the signal-to-noise ratio, which significantly improves the quality of the developed reconstruction algorithm [50]–[52]. An ECT sensor with 12 electrodes is selected since It is known that the number of electrodes has a direct relationship with the signal-to-noise ratio.

The flask is earthed to eradicate external noises and stray capacitance effects [53]. Grounded guards are uniformly placed between the electrodes to increase the sensors' dynamic range and keep the electrical field uniform. For a certain metal distribution, the corresponding mutual capacitance measurements are sequentially collected by activating one electrode at a time as a transmitter, while all other electrodes are grounded to work as receivers. Therefore, the number of independent capacitance measurements M for one distribution is computed as in the following Eq.1:

$$M = \frac{n(n-1)}{2} \quad (1)$$

A. ECT MODEL

The ECT model consists of forward and inverse problems. The solution of the forward problem requires building a FEM to determine the capacitance measurements for a certain metal distribution. Fig. 5b shows the FEM of the ECT system. The area of the foam pattern, where the metal will exist, is divided into $16 \times 16 = 256$ elements. The number of all other elements equals 4364. The change of the metal distribution has a nonlinear effect on the capacitance measurements as described in the following Laplace Eq.2

$$\Delta \cdot (\varepsilon \Delta u) = 0 \quad (2)$$

where ε is the permittivity of the materials distribution, and u is the electrical potential. Since the material distribution in the LFC application is grounded metal, the boundary condition for solving Eq.2 are given as follow [26]:

$$\omega^i = \begin{cases} V_c & (x, y) \subseteq \Gamma_i \ (i = 1, 2, \cdots 12) \\ 0 & (x, y) \subseteq \Gamma_k + \Gamma_s + \Gamma_g + \Gamma_e \end{cases} \quad (3)$$

where V_c is the excitation voltage, Γ_i is the surface of the transmitting electrode $i = 1, 2, \cdots 12$, Γ_k is the surface of the receiving electrodes $k = 1, 2, \cdots 12$, Γ_s and Γ_g are the surfaces of the grounded flask and the guards between electrodes, respectively, and Γ_e represents the surface of the elements where the grounded metal will exist inside the imaging area.

Equation 2 can be numerically solved based on the developed FEM in Fig. 5b. Therefore, the linear forward solution of the ECT is described as:

$$C_{M \times 1} = S_{M \times N} \cdot G_{N \times 1} \quad (4)$$

(a) Cross-sectional view of ECT system
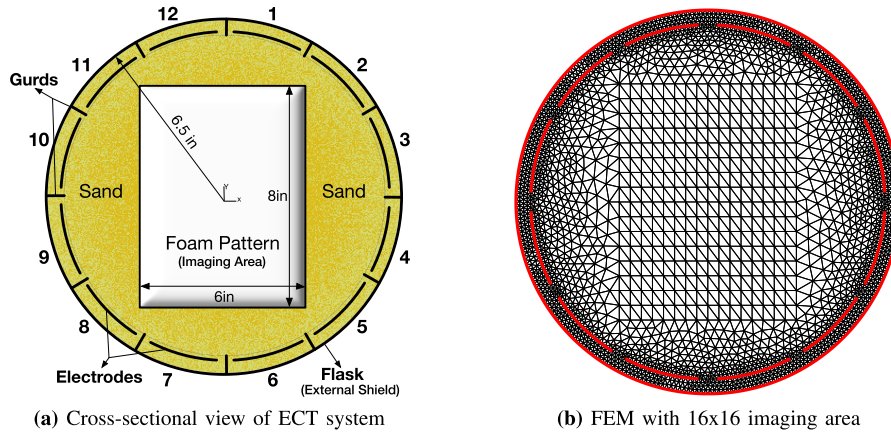
(b) FEM with 16x16 imaging area

FIGURE 5. ECT system with 12 electrodes.

where C is the measurements vector, G is the image of the metal distribution, N the number of images' pixels, and S is the sensitivity matrix calculated for each element k as follows:

$$S_{i,j}(k) = \frac{C_{i,j}(k) - C_{i,j}^l}{C_{i,j}^h - C_{i,j}^l} \quad (5)$$

where $C_{i,j}^h$ are capacitance when the imaging region is entirely foam and $C_{i,j}^l$ are capacitance when the foam completely replaced by metal.

The ECT is an ill-posed problem, since $N \gg M$. Therefore, the reconstructed image's error can significantly affect any small change in the measurements [54]. There are two types of image reconstruction algorithms, non-iterative and iterative. The non-iterative algorithms, such as Linear Back Projection (LBP) Eq.6, are simple but generate low-quality images.

$$G = S^T C \quad (6)$$

While applying the Landweber iterative algorithm, Eq.7 significantly improves the image quality but applies high computations.

$$G_{k+1} = G_k - \lambda S^T (SG_k - C) \quad (7)$$

where λ is the relaxation parameter, SG^k is the forward problem solution, and k is the iteration number [54].

### B. COMPUTATIONAL PROBLEMS OF THE ECT SYSTEM FOR LFC PROCESS

In the wider context, many key problems present a serious challenge to the implementation of the ECT system [55]. The main reasons that are presented to an implementation of the ECT system are Soft fields, Ill-posed, Nonlinearity. Beside, practically imaging conductive materials by placing a grounded conductor in the imaging area dramatically affects the linear sensitivity matrix [47]. Therefore, solving the inverse problem using the traditional ECT algorithms, such as LBP, Landweber, or iterative Tikhonov, produces

poor images. Improving the reconstructed images using these traditional algorithms requires updating the sensitivity matrix each iterations which consumes much time and makes these algorithms are not feasible in dynamic applications such as the LFC process. For illustrating, the linear sensitivity is computed when the imaging area is empty, while the actual sensitivity is computed when a piece of grounded metal is placed inside the imaging area. Fig 6 shows how much the grounded metal inside the imaging area deforms the values of the linear sensitivity matrix. The sensitivity between electrodes (2-8) are shown in Fig. 6b, and in Fig. 6c between electrodes (2-7). Fig. 6 proves that applying the linear sensitivity matrix in the ECT system for imaging grounded conductive materials generates poor images. Besides, computing the actual sensitivities during iterations is time-consuming. Therefore, building novel reconstruction algorithms that do not use the sensitivity matrix is crucial.

To address these challenges, multivariate, complex, and unforeseeable operating conditions demand better modeling, description, understanding, and interpretation by monitoring and controlling industrial systems' dynamic behavior. In addition to the techniques mentioned above to develop image reconstruction algorithms, a new technology that has newly gained a significant momentum is Deep Learning (DL) [56]. This new technique forms a category of machine learning computational area, which is analogous to ANN. As deep neural networks have shown a very astonishing success, often further than human capacities, in solving challenging problems with remarkable accuracy in many contemporary studies and various domains such as medical [57], and industry [58]. These profound findings of DL triggered us a broad interest in using these techniques to address both the forward and inverse problems of the ECT system for an industrial process.

III. DEEP LEARNING
Deep learning is a spectacular division of Artificial Intelligence (AI) and, in particular, Machine Learning (ML), which has achieved great success in past and present periods in
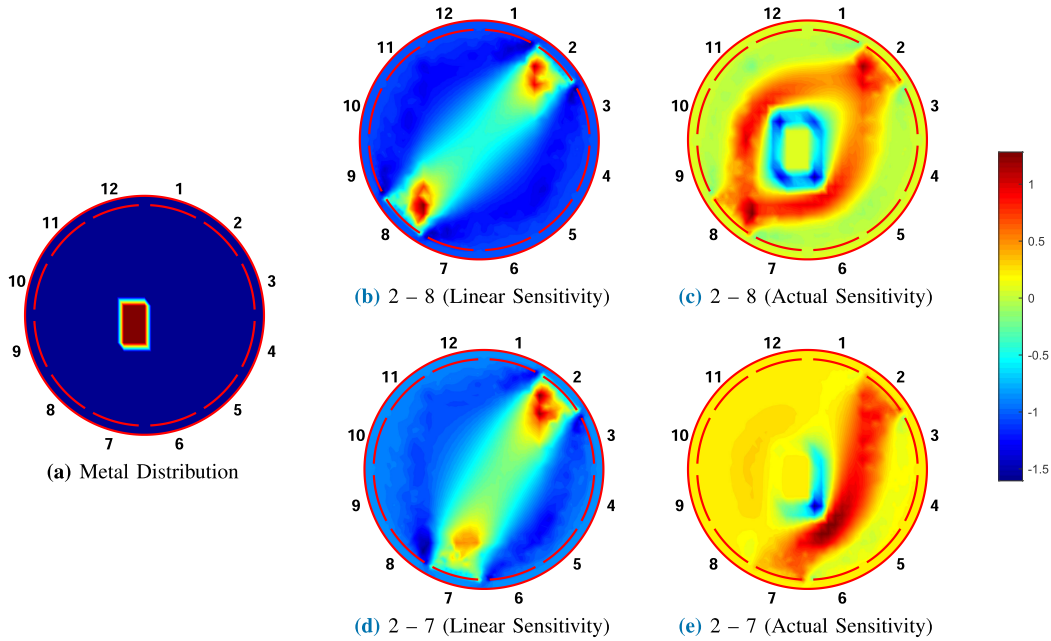
FIGURE 6. Linear and actual sensitivity matrices for electrode pairs (2-8) (b & c), (2-7) (d & e) for a single piece of metal (a).

varied fields of science and applications such as in medical applications [59], agriculture applications [60], business [61], industry [62] and government [63]. Deep Neural Network (DNN), Convolutional Neural Network (CNN), and Recurrent Neural Network (RNN) are examples of the DL models.

RNNs are neural networks with recurrent links between the hidden nodes of the hidden layers. These cyclical connections provide RNNs the capacity to encode memory, and as that these RNNs, if prosperously trained, are proper for sequence learning applications. Long Short Term Memory (LSTM)-RNN [64] is a novel RNN network design. The LSTM is a customary RNN where the monotonic nonlinearity, such as the sigmoid or tanh, is commuted with a memory module that can expeditiously save continuous values and transfer information long temporal range. Every memory module in the LSTM of RNN has a property of constant linear dynamics with a feedback loop with a weight of one unit. As an upshot, the error signal does not decay or explode as it propagates over the memory module. The memory's cell content is adjusted by several gates that confer the LSTM unit the power to hoard and restore the pertinent series information. However, with more various gates be added to the LSTM architecture, the network's complexity will be increased.

Due to our desire for the low complexity of RNN models and the promising results arrived at by the LSTM-RNNs networks in several domains, we thence directed our attention to the LSTM-RNNs to explore its importance in the ECT from a dynamical manufacturing system perspective.

IV. ECT-LSTM-RNN: FORWARD AND INVERSE PROBLEMS SOLVER

This work's contribution is the evolution of an image reconstruction model for the distribution of metal filling for the LFC process based on ECT using advanced deep learning methods. The distinction between convolutional layers is made by their capability to retrieve useful knowledge and learn the internal representation of time-series data. At the same time, LSTM networks are efficient in identifying short-term and long-term dependencies. The proposed model's basic idea in this research is to incorporate these deep learning techniques' merits effectively. In this respect, the proposed model, called LSTM-RNN, comprises of two main components, as shown in Fig. 7: The first component composes of convolutional and pooling layers in which complex mathematical calculations are conducted to incubate the features of the input data. The second component exploits the features created by the LSTM and dense layers. After that, we provide a brief description of the convolutional, pooling, and LSTM layers that form the proposed model's heart.

A. CONVOLUTIONAL AND POOLING LAYERS

Convolutional and pooling layers [65] are principally designed pre-processing data layers that have the job of filtering the input data and extracting useful information that would typically be used as input a fully connected network layer, as shown in Fig. 7. More characteristically, the convolutional layers use convolution operation between raw input data and convolution kernels to yield new values for the features. The input data should contain a structured matrix form since this technique was primarily purposed to extract features from image data sets [66]. The convolution kernel (i.e., the filter) can be thought of as a tiny window (compared to the input matrix) which has coefficient values into a matrix form. This window slides throughout the input matrix and applies convolution operation on each sub-region (i.e., patch) that this specific window meets across the input matrix. The outcome
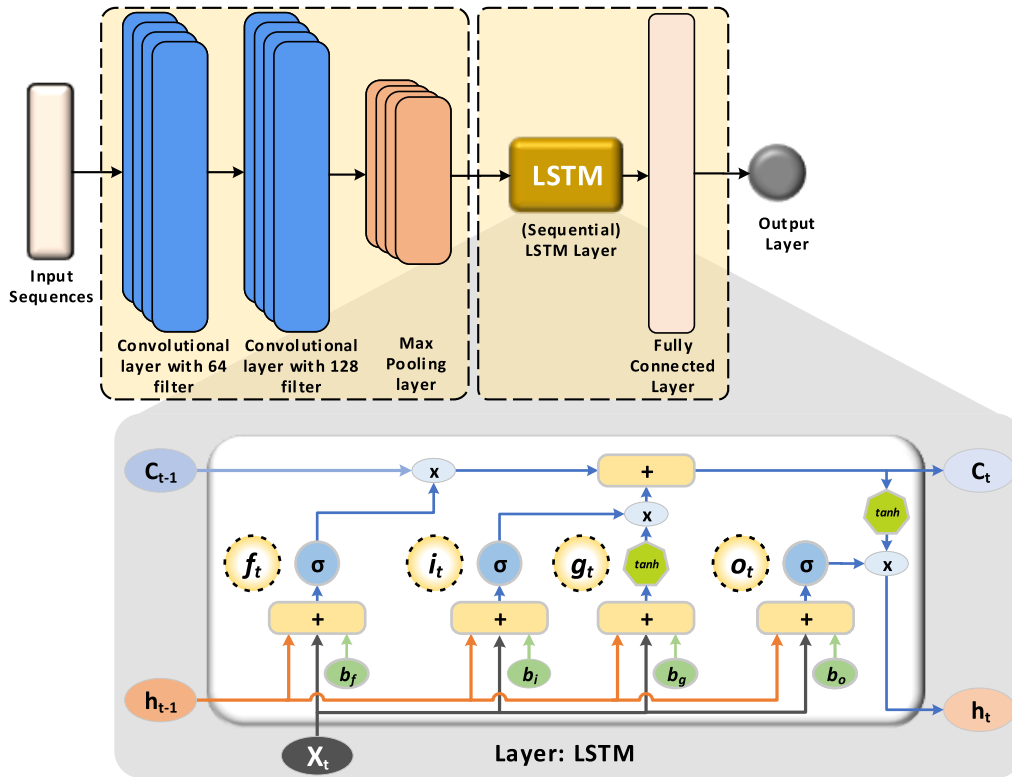
FIGURE 7. Architecture of a long short-term memory (LSTM).

of all these operations is a convolved matrix representing the value of a feature defined by the coefficient values and the dimension size of the used filter. By applying different convolution kernels on the input data, many convolved features can be created, which are customarily more beneficial than the original initial features of the input data, thus improving the performance of the model. Typically, the convolutional layers are followed by a non-linear activation function, such as a rectified linear unit, and then a pooling layer. A pooling layer is a sub-sampling method that extracts specific values from the convolved features and generates a matrix with lower dimensions. By an analogous procedure, as with the operations performed on the convolutional layer, the pooling layer uses a small sliding window that uses the values of each patch of the convolved features as input and produces one new value as an output that is determined by an operation that the pooling layer is defined to perform. The maximum pooling and average pooling compute the maximum and average value of the values of each patch. As an outcome, the pooling layer leads up to new matrices. These matrices can be deemed as short versions of the convolved features produced by the convolutional layer. The pooling process can help the system be more potent because tiny input changes will not alter the pooled values of the output.

B. LSTM LAYERS
LSTM neural networks [64] are a particular kind of Recurrent Neural Networks (RNNs), which can learn long-term dependencies out of the use of feedback connections. Classical RNNs seek to find a solution for feedforward NNs, called "lack of memory," which is accountable for showing a low level of performance on sequences and time-series datasets. These models use periodic interrelatedness on their hidden layer to get short-term memory and capture information from sequences and time-series datasets. However, RNNs suffer from the common vanishing gradient problem that shackles the model for learning long-range dependencies. LSTM addresses this problem by stowing practical information on memory cells and fading away needless information, thus realizing, generally, a better overall performance than a traditional RNN.

Each LSTM consists of a memory cell in addition to three main gates: i-input, f-reset (forget), g-cell candidate, and o-output. Through this architecture, the LSTM was able to generate a controlled information flow by defining which information should be "forgotten" and which should be "remembered," thus managing the learning of long-term dependencies. In further detail, the input gate, i_t, alongside the second gate g_t, manages the new extracted information that is cached into the memory state g_t at time t. The forget gate, or called f_t, controls the previous information that should either disappear or should be preserved in the memory cell at time $t-1$. The output gate o_t manages the information that could be used for the memory cell's output. In summary, Equations 9 - 13 briefly characterize the operations implemented by the LSTM unit.

Weights W, the recurrent weights R, and biases b can be described by Formula 8.

$$W = \begin{bmatrix} W_i \\ W_f \\ W_g \\ W_o \end{bmatrix}, \quad R = \begin{bmatrix} R_i \\ R_f \\ R_g \\ R_o \end{bmatrix}, \quad b = \begin{bmatrix} b_i \\ b_f \\ b_g \\ b_o \end{bmatrix} \quad (8)$$

where i, f, o, and g denote the input, forget, output gates, and cell candidate, respectively.

$$i_t = \sigma(W_i x_t + R_i h_{t-1} + b_i), \quad (9)$$
$$f_t = \sigma(W_f x_t + R_f h_{t-1} + b_f), \quad (10)$$
$$o_t = \sigma(W_o x_t + R_o h_{t-1} + b_o), \quad (11)$$
$$g_t = tanh(W_g x_t + R_g h_{t-1} + b_g), \quad (12)$$
$$c_t = g_t \odot c_{t-1} + i_t \odot g_t, \quad (13)$$

where $\odot$ stands for component-wise multiplication operator, x_t stands for the input gate, and σ is a sigmoid function, which can be expressed by $\sigma(x) = (1 + e^{-x})^{-1}$. The h_t represents the hidden state that comprises the memory cell's output that can be computed by:

$$h_t = o_t \odot tanh(c_t) \quad (14)$$

Note that if multiple LSTM layers are stacked together, the hidden state, called h_t, and the memory state, called c_t, of each LSTM layer is forwarded as inputs following the LSTM layer.

C. ECT-LSTM-RNN MODEL

The LSTM most works with time sequences, however LSTMs are just a part of the deep architecture, whose top layer can do anything, including simply compute a nonlinear function of its features, whose squared error is minimized vs a continuous target variable. LSTMs do not always need to predict the next step in a sequence, instead we can feed whatever output we expect. In the implementation developed in this work, the proposed ECT-LSTM-RNN model consisted of 2 convolutional layers of 64 and 128 filters, respectively, where each layer's size is 2. These layers are then followed in sequence by a max-pooling layer with a maximum 2, an LSTM layer, a dense layer containing 32 neurons, and an output layer consisting of a single neuron. Fig. 7 presents the architecture of the proposed ECT-LSTM-RNN model.

V. EXPERIMENT SETUP AND RESULTS
A. ECT-LSTM-RNNs SOLVER FOR THE FORWARD PROBLEM

In this work, a deep learning solution to the forward problem is presented. Deep knowledge of the ECT system, as well as the LFC process, is crucial. In the ECT system, the forward problem solution computes the capacitance data, C_{uv}, between electrodes u and v for certain material's distribution, $\varepsilon(x, y)$.

The capacitance is calculated for each pixel between all the electrodes after filling that pixel by metal and keeping the rest empty. The filled pixels are represented by one, while the empty are zeros. The produced normalized capacitance are saved in the *sensitivity matrix* (S). The capacitance can be linearized, where the metal distribution domain is split into $k \times k$ pixels, as presented in Eq. 15.

$$C = \sum_{u=1}^{k} \sum_{v=1}^{k} S_{uv} G_{uv}. \quad (15)$$

In Equation 15, it is presumed that the distribution of the electric field does not alter the various material distribution function, where the pixels linearly influence capacitance measurements. The linearized solution of the Eq. 15 is reached by a linear superposition of the varied elements of the S weighted by G.

Firstly, ANSYS Finite Element (FE) software is applied to build the ECT forward model. This model takes predefined metal distribution as input and calculates its corresponding capacitance measurements as output [43].

B. DATA SETS GENERATION

In the LFC process, the molten metal decomposes a foam pattern and produces the final cast. The position of the metal during the casting simulates the training data generation. There are three physical mechanisms of the foam decomposition which differ based on different factors. Two main factors are the foam beads type and the gate's location where the metal enters the pattern [69]. There are three modes of the foam decomposition, Contact, Gap, and Collapsed [41]. We have used these modes to simulate the metal's characteristics during the casting process, and created the required training and testing date sets.

1) **Contact mode** (Fig. 8(a)), the molten metal gradually flows and pushes against the foam,
2) **Gap mode** (Fig. 8(b)), polymer vapor causes an air gap between the metal and the foam,
3) **Collapse mode** (Fig. 8(c)), the liquid metal takes random directions, like fingers, because of the foam joining inter-bead.

Imaging conductive materials using ECT technique entirely differs than the typical ECT for non-conductive materials. The grounded metal decomposes the foam and works as a shield between the transmitters and receivers. In the three decomposition modes, there is no such effect on the measurements by dielectric constant of the decomposed foam. We have built an FEM model to simulate the movement of the grounded metal and the decomposition modes. Typically, the capacitance measurements are computed and normalized as given in Eq.16.

$$C_N = \frac{C_i^E - C_i}{C_i^E - C_i^M} \quad (16)$$

where C_i^E and C_i^M are measurements when the imaging area is empty and filled by the metal, respectively, C_i is the measurement vector corresponding to a known metal distribution. Fig. 9 illustrates the contact decomposition mode, and
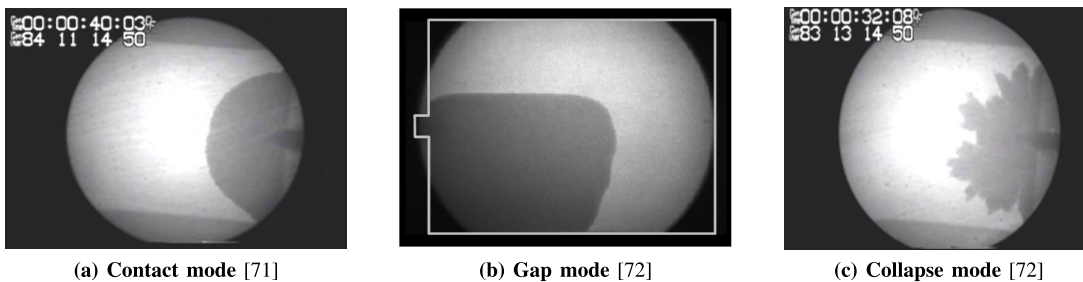
(a) Contact mode [71]   **(b) Gap mode [72]**   **(c) Collapse mode [72]**

FIGURE 8. **Different types of foam decomposition.**
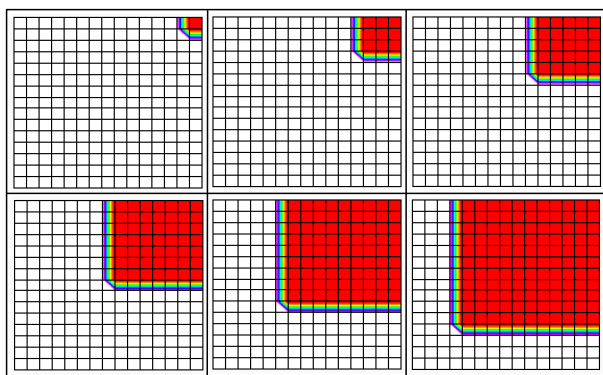
FIGURE 9. **Metal distributions simulating the contact mode.**
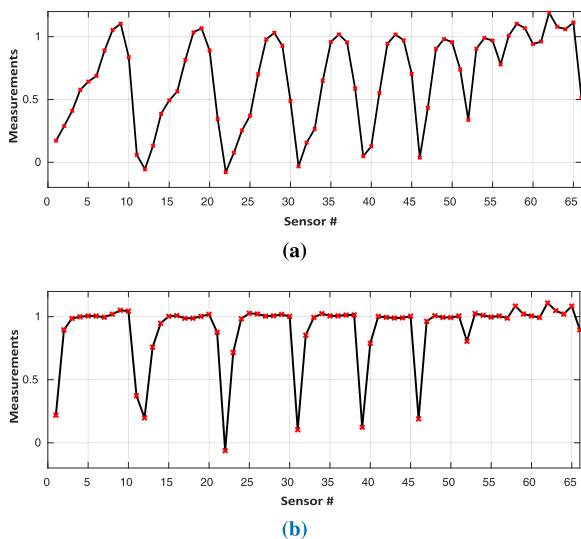

(a)

(b)

FIGURE 10. **Normalized capacitance measurements of (a) Second metal distribution (b) Last metal distribution in Fig. 9.**

normalized measurements of the second and last distributions are shown in Fig. 10.

The ANSYS mimics cylindrical vessel contains a metal cub surrounded by a dialectical material (sand). The vessel is surrounded by twelve plates, measuring 66 readings, as shown in Fig. 5a. The simulation models different positions and sizes of the metal cube. The cross-sectional image appears as a metal square. The data consists of 996 examples, with 784 for training and 212 for evaluation according to the

original experiment [23], unlike other datasets that contain millions of images such as image net. The data set contains only hundreds of examples, but it is sufficient enough to conduct the experiment where the problem at hand is much more constrained, it has specific physical laws, and it has much less variability than, for example, image recognition.

C. VALIDATION CRITERION

A nominal validation criterion is presented to estimate the distribution of metal fill in Eq. 17.

$$IE = \frac{||G - \hat{G}||}{||G||} \quad (17)$$

where *IE* refers to an image normalized error, $\hat{G}$ represents the predicted grounded metal distribution from the image reconstruction process based DL models, and *G* represents the original grounded metal distribution.

D. RESULTS OF THE FORWARD PROBLEM

Figs. 11 and 12 show respectively the training and prediction capacitance measurement results with the ECT-LSTM-RNN in the forward problem for a metal filling distribution of an LFC process using 66 measurements. It is observed from Figs. 11 and 12 that there is a high degree of response for the ECT-LSTM-RNN for a metal filling distribution of an LFC process. The convergence curve, of the performance of the proposed model, for the forward problem in the ECT problem for a metal filling distribution of an LFC process, are presented for up to 1800 iterations in Fig. 13. The convergence curve shows that ECT-LSTM-RNN provides a stable estimate of the 66 measurements. The normalized errors in both training and testing cases of ECT-LSTM-RNN forward problem solver are drawn in Fig. 14 and Fig. 15, respectively.

Figs. 14 and 15 are considered to assess the efficiency of LSTM-RNN by showing the normalized errors for the 66 measurements of metal filling distribution. The converged train and test normalized errors in the forward problem are respectively reported as 0.0380 and 0.0571. These low error rates support that the approach of ECT-LSTM-RNN for metal filling distribution achieved small error rates. Table 1 shows the normalized error for the three different foam decomposition modes of the testing patterns. The normalized error for the collapsed mode is higher than the other two modes.
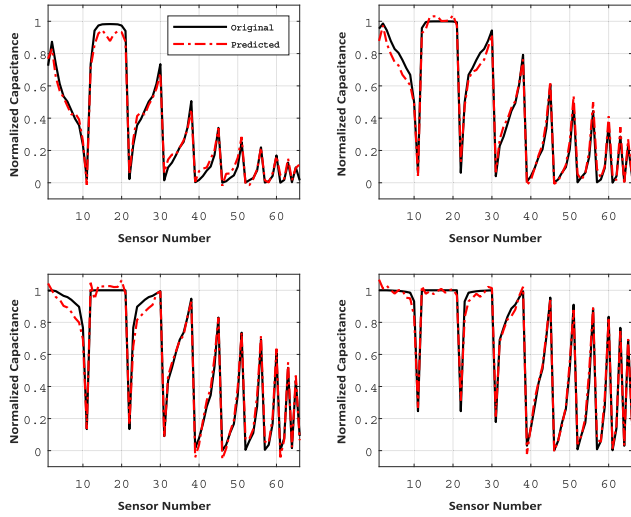
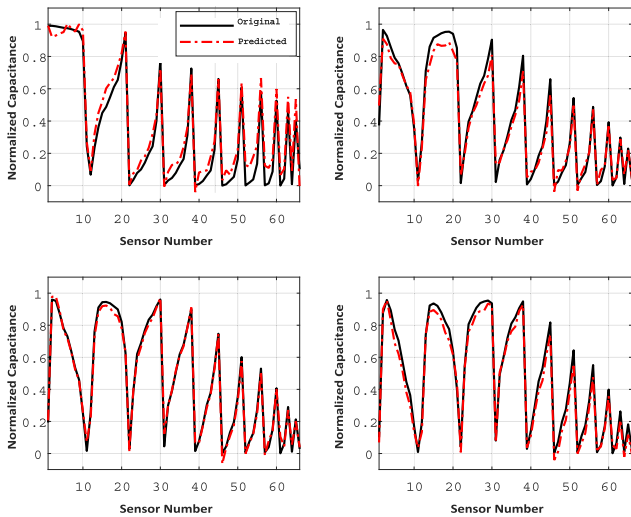**FIGURE 11.** Forward Problem: Original and Predicted Capacitance Measurements in Training Case.

FIGURE 12. Forward Problem: Original and Predicted Capacitance Measurements in Testing Case.

TABLE 1. Normalized error of testing patterns for forward problem.

Decomposition Mode	Contact	Gap	Collapsed
Normalized Error	0.0114	0.0142	0.0315

E. ECT-LSTM-RNNs SOLVER FOR THE INVERSE PROBLEM

The inverse problem is defined as the process of locating an inverse relationship, in which the capacitance data is used to compute the distribution of the material, and as a consequence, a visual image is generated by a reconstruction method. Equation 18 is given to represent such an inverse relationship.

$$G(x, y) = F^{-1}(C_{12}, \ldots, C_{uv}, \ldots, C_{K-1,K}) \qquad (18)$$

F. EXPERIMENTAL SETUP

Real experiments of the LFC requires working in a very harsh environment inside a foundry with very hot molten metal.
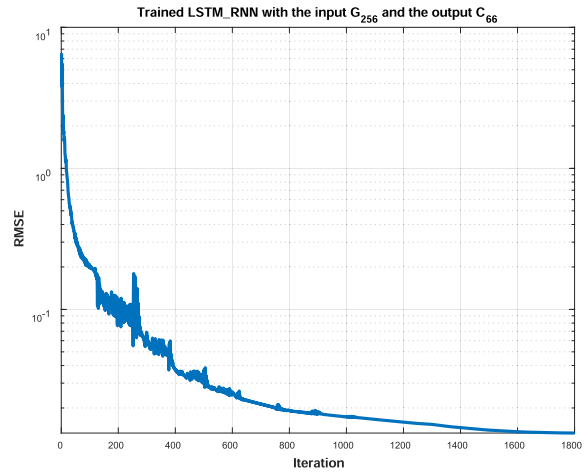

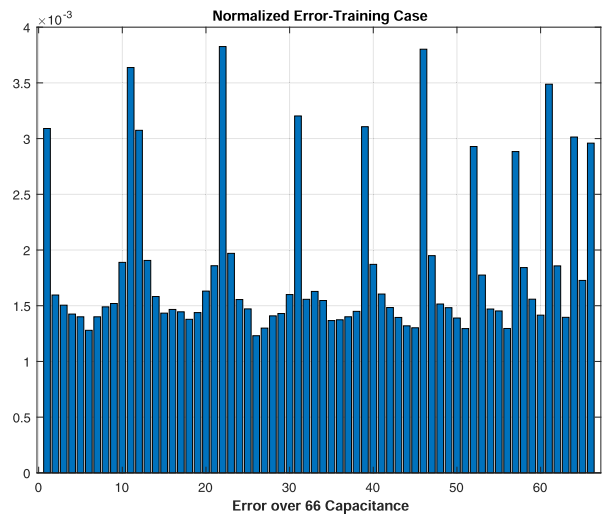**FIGURE 13.** Forward Problem: Training Convergence Curves.

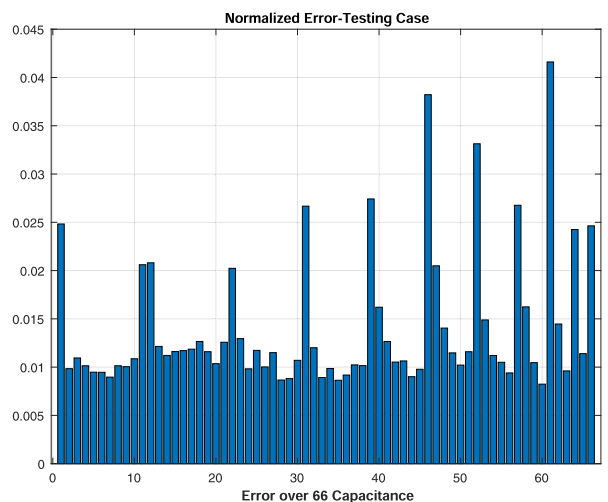**FIGURE 14.** Forward Problem: Normalized Error in training cases.
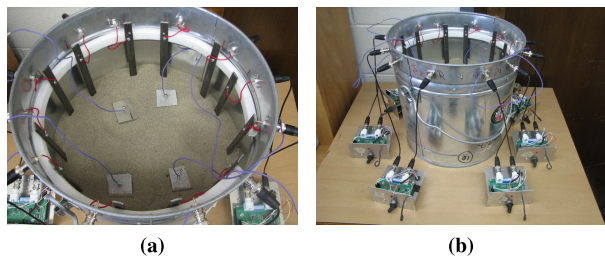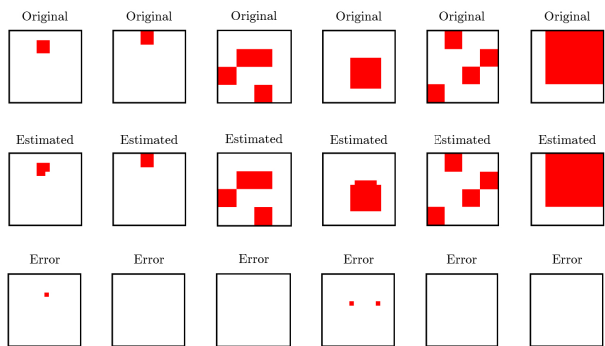

FIGURE 15. Forward Problem: Normalized Error in testing cases.

Earlier, we developed the real foundry environment and published our results in [50], [51]. For testing purposes, an ECT

FIGURE 16. Images of the actual ECT model show the wireless sensors in (a) and the distribution of the sensors around 4 pieces of metal in (b).
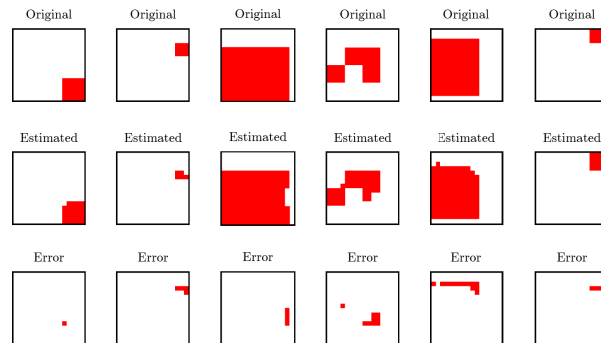

FIGURE 17. Inverse Problem: Original and Predicted Images in Training Case.

FIGURE 18. Inverse Problem: Original and Predicted Images in Testing Case.

FIGURE 19. Inverse Problem: Training Convergence Curve.

FIGURE 20. Inverse Problem: Normalized Error in training cases.

tomography system was developed for simulating the casting process in the lab. Fig. 16a shows the ECT system consisting of a cylindrical tube (flask) with 12 electrodes mounted on its circumference. There are four metal pieces placed in the four corners of the imaging area, where the foam pattern should exist. The capacitance are measured between these electrodes in a sequence by connecting one electrode in a time to the source signal and the others to the earth. Fig. 16b illustrates the electronic measuring circuits connected to Motes wireless transmitters which send the measured data to a base station where the proposed image reconstruction algorithm is implemented.

The measuring circuits are controlled by a LabVIEW program implemented on the base station. The program collects the measurements, and processes it to be appropriate for the reconstruction algorithm. The distance between the metal and the sensors changes the range of capacitance measurements. For instance, the normalized capacitance values from one sensor will be very high when the metal is placed very close to it. Meanwhile, the readings from the adjacent sensors will be almost half, and the others from far sensors will be small.

Figs. 17 and 18 illustrate the potential capability of the ECT-LSTM-RNN in the inverse problem in training and testing, respectively for a metal filling distributions. One piece of metal represents either Contact or Gap modes where there is a continuity of the metal's flow, and two pieces or more characterizes the Collapsed mode where the metal scattered in the filling area.

The performance of the proposed system for the inverse problem for a metal filling distribution of an LFC process problem is shown, for up to 1800 epochs, in Fig. 19.
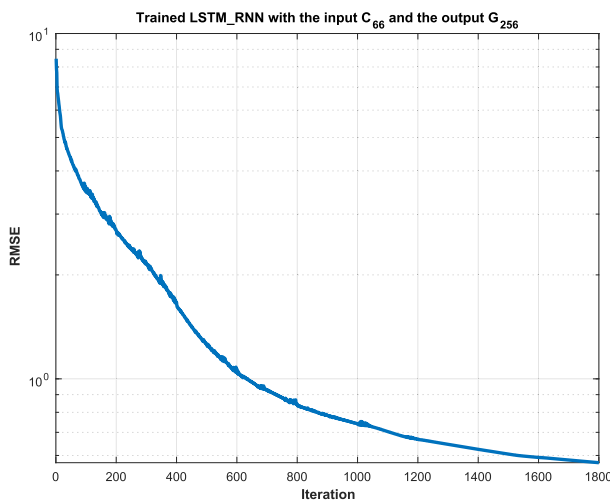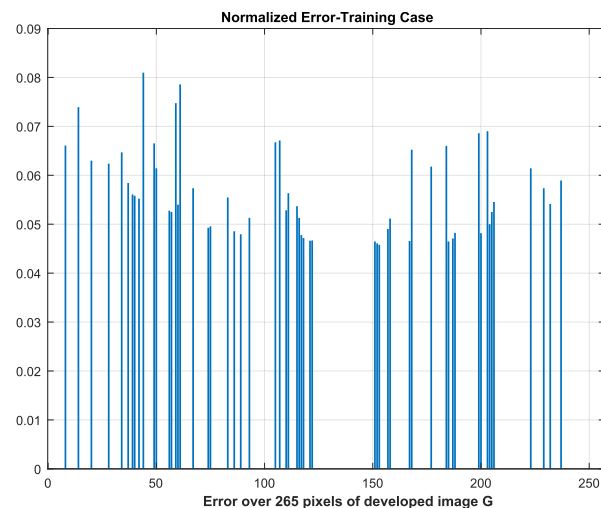
In Fig. 19, the search based ECT-LSTM-RNN in the inverse problem converges rapidly and reliably. The normalized errors in both training and testing phases in the inverse problem metal filling distribution are shown in Figs. 20 and 21.

The train and test normalized errors in the ECT problem's inverse problem are reported as 0.025 and 0.0929,

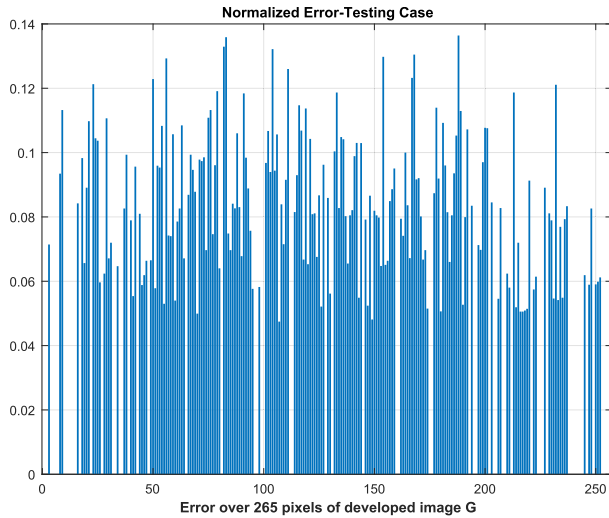**FIGURE 21.** Inverse Problem: Normalized Error in testing cases.

TABLE 2. Normalized error of testing patterns for inverse problem.

Decomposition Mode	Contact	Gap	Collapsed
Normalized Error	0.0215	0.0232	0.0482

TABLE 3. Results of the IE of different ECT image reconstruction algorithms.

	Phantom	LBP	Tikhonov	ECT-LSTM-RNN
	1	0.6280	0.8670	0.0000
	2	0.8225	0.7301	0.0000
	3	0.7919	0.7325	0.0000
	4	0.8238	0.6961	0.1925
Relative	5	0.7233	0.7580	0.0000
Image	6	0.9135	0.8875	0.0000
Error	7	0.8307	0.7918	0.1741
	8	0.8262	0.7769	0.0000
	9	0.8363	0.9233	0.1260
	10	0.8455	0.8125	0.2582

TABLE 4. Reconstruction time in sec.

Algorithm	LBP	Tikhonov	ECT-LSTM-RNN
Time	0.086	6.5357	0.152

respectively. These lowest normalized error rates illustrate that the ECT-LSTM-RNN achieved a high-performance level for a metal filling distribution in the inverse problem. Table 2 shows the normalized error for the three different foam decomposition modes. The normalized error for the collapsed mode is higher than the other two modes.

G. COMPARISON WITH REGULAR IMAGE RECONSTRUCTION ALGORITHMS

A comparison between the proposed ECT-LSTM-RNN algorithm and other well defined ECT image reconstruction algorithms is carried out to compare the performance and the quality of the reconstructed images. A variety of distribution patterns were set up to test the generalization ability of the proposed model. The results are shown in Fig. 22, where the first column represents the distribution of the real material, and the rest columns containing the reconstructed images from the LBP, iterative Tikhonov, and ECT-LSTM-RNN algorithms, respectively. The Tikhonov iteration number is 1000 iterations. The results of the ECT-LSTM-RNN algorithm have high quality and accuracy with sharp objects' boundaries compared with the reconstructed images from the LBP, and iterative Tikhonov algorithms. Visually, it is clear from the results in Fig. 22 that the object edges are clear since there is no transition zone between the reconstructed objects by the proposed algorithm compared with the other algorithms. Also, the results of the IE measure stated in Table 3 prove that the performance of the ECT-LSTM-RNN algorithm is better than other reconstruction algorithms.

Typically, imaging speed is a vital evaluation measure for reconstruction algorithms. For the experimental capacitance data, the imaging costs of different algorithms are stated in Table 4. The calculations are carried out using a PC with an i9 CPU (3.6 GHz) and 32 GB memory. The imaging cost of our method is 0.152 seconds, which is much smaller than 6.53 seconds with iterative Tikhonov method. Our method is faster and construct more accurate images compared to the other iterative methods. Although the LBP is faster than our proposed method, the image qualities are much lower than our method.

H. RESULTS OF NOISY DATA

The robustness and generalization of the proposed ECT-LSTM-RNN inverse solver is tested by using artificial noisy data during the training and testing phases. The dataset is randomly divided into a training set with ratio 70% and the rest 30% as testing set. Afterwards, artificial Gaussian noise with Signal to Noise Ratio (SNR) equals 30dB is added to the capacitance input vectors of training and testing datasets. The ECT-LSTM-RNN inverse solver is separately trained and tested with original noise-free and noisy training and testing dataset, respectively. Table 5 shows the comparing results of the minimum, maximum and average of normalized image error for different types of data. The statistics values in Table 5 show that the trained ECT-LSTM-RNN model with noise-free training dataset performs with better average normalized image error on the noise-free testing dataset compared with the other testing data with noise. In the meantime, the performance measures of the trained network with noisy data are little bit worse than those of training
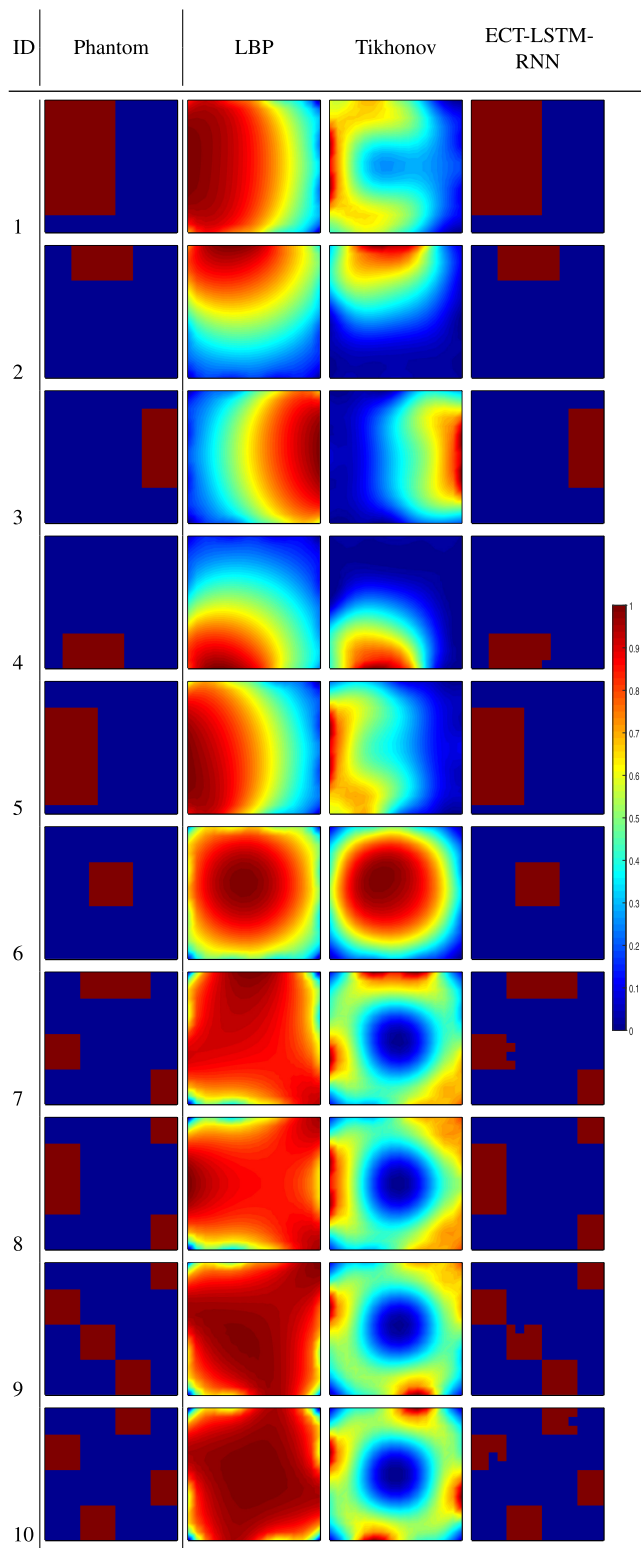
FIGURE 22. Reconstructed images of different commonly used image reconstruction algorithms.

TABLE 5. Results of noise-free and noisy training and testing data.

Training Data		Noise-Free		Noisy	
Testing Data		Noise-Free	Noisy	Noise-Free	Noisy
Normalized Image Error	Min	0.0391	0.0430	0.0434	0.0444
	Max	0.1482	0.1659	0.2131	0.2255
	Avg.	0.0929	0.1035	0.1185	0.1253

noise in terms of certain specific image reconstruction examples.

VI. CONCLUSION

Electrical Capacitance Tomography (ECT) is a flexible and low-cost method as well that could be adapted simply too old/new systems such as oil or gas pipelines. However, poor image quality limited their usage. This paper investigates a deep neural network model; herein we used the Long Short-Term Memory Recurrent Neural Network (LSTM-RNN) models to solve the main forward and inverse problems for ECT technology in the lost foam casting process. The proposed two models have achieved high accuracy results. It is well known that neural nets impute data/information but training crucial to obtain accurate results. It is challenging to interpret how a neural network employs all the imputed information, but the physical nature of the problem makes it much more possible to deduce an accurate mapping that converts surface measures into vessel internal image.

REFERENCES

[1] Y. Chen, K. Li, and Y. Han, "Electrical resistance tomography with conditional generative adversarial networks," *Meas. Sci. Technol.*, vol. 31, Dec. 2019, Art. no. 055401. [Online]. Available: https://iopscience.iop.org/article/10.1088/1361-6501/ab62c4

[2] R. Harikumar, R. Prabu, and S. Raghavan, "Electrical impedance tomography (EIT) and its medical applications: A review," *Int. J. Soft Comput. Eng.*, vol. 3, no. 4, pp. 193–198, 2013. [Online]. Available: http://scholar.google.com/scholar?hl=en&btnG=Search&q=intitle:Electrical+Impedance+Tomography+(+EIT+)+and+Its+Medical+Applications+:+A+Review#0

[3] M. Neumayer, H. Zangl, D. Watzenig, and A. Fuchs, "Current reconstruction algorithms in electrical capacitance tomography," in *New Developments and Applications in Sensing Technology* (Lecture Notes in Electrical Engineering), vol. 83. Berlin, Germany: Springer, 2011, pp. 65–106. [Online]. Available: http://link.springer.com/10.1007/978-3-642-17943-3_4

[4] N. A. A. Rahman, R. A. Rahim, A. M. Nawi, L. P. Ling, J. Pusppanathan, E. J. Mohamad, C. K. Seong, S. M. Din, N. M. N. Ayob, and F. R. M. Yunus, "A review on electrical capacitance tomography sensor development," *J. Teknol.*, vol. 73, no. 3, 3 2015. [Online]. Available: http://www.journalteknologi.utm.my/index.php/jurnalteknologi/article/view/4244

[5] M. A. Abdelrahman, A. F. Sheta, and W. A. Deabes, "Fuzzy mathematical modeling for reconstructing images in ECT of manufacturing processes," in *Proc. Int. Conf. Comput. Eng. Syst.*, Dec. 2009, pp. 461–468.

[6] C. E. Agu, A. Ugwu, C. Pfeifer, M. Eikeland, L.-A. Tokheim, and B. M. E. Moldestad, "Investigation of bubbling behavior in deep fluidized beds at different gas velocities using electrical capacitance tomography," *Ind. Eng. Chem. Res.*, vol. 58, no. 5, pp. 2084–2098, Feb. 2019.

data without noise, but still substantial. Statistics in Table 5 show that image reconstruction results are not much different indeed, and results of training and testing data with noise may not be worse than that of training and testing data without

[7] M. B. Haddadi and R. Maddahian, "A new algorithm for image reconstruction of electrical capacitance tomography based on inverse heat conduction problems," *IEEE Sensors J.*, vol. 16, no. 6, pp. 1786–1794, Mar. 2016.

[8] A. Korjenevsky, "Electric field tomography for contactless imaging of resistivity in biomedical applications," *Physiol. Meas.*, vol. 25, no. 1, p. 391, 2004.

[9] T. Rymarczyk, G. Káosowski, and E. Kozáowski, "A non-destructive system based on electrical tomography and machine learning to analyze the moisture of buildings," *Sensors*, vol. 18, no. 7, p. 2285, Jul. 2018.

[10] M. Takei, D.-H. Doh, and M. Ochi, "Electrical CT image reconstruction technique for powder flow in petroleum refinery process," *Experim. Fluids*, vol. 44, no. 3, pp. 481–490, Mar. 2008.

[11] M. Wang, *Industrial Tomography: Systems and Applications*. Amsterdam, The Netherlands: Elsevier, 2015.

[12] W. Deabes and M. Abdelrahman, "Solution of the forward problem of electric capacitance tomography of conductive materials," in *Proc. 13th World Multi-Conf. Systemics, Cybern. Inform.*, vol. 4, 2009, pp. 1–5.

[13] G. Yanli, X. Qing, L. Kunming, and G. Junjie, "Overview on image reconstruction algorithms for electrical capacitance tomography," in *Proc. 37th Chin. Control Conf. (CCC)*, Jul. 2018, pp. 3405–3411.

[14] T. Wondrak and M. Soleimani, "A novel metal flow imaging using electrical capacitance tomography," *Meas. Sci. Technol.*, vol. 28, no. 6, 2017, Art. no. 064001. [Online]. Available: http://stacks.iop.org/0957-4484/29/i=34/a=342001

[15] X. Liu, X. Wang, H. Hu, L. Li, and X. Yang, "An extreme learning machine combined with Landweber iteration algorithm for the inverse problem of electrical capacitance tomography," *Flow Meas. Instrum.*, vol. 45, pp. 348–356, Oct. 2015, doi: 10.1016/j.flowmeasinst.2015.07.009.

[16] Q. M. Marashdeh, F. L. Teixeira, and L.-S. Fan, "Adaptive electrical volume tomography," *IEEE Sensors J.*, vol. 14, no. 4, pp. 1253–1259, May 2014.

[17] Z. Zeeshan, F. L. Teixeira, and Q. M. Marashdeh, "Fast algorithm for image reconstruction in adaptive electrical capacitance tomography," in *Proc. IEEE Sensors*, Dec. 2017, pp. 1–3.

[18] Y. Li and W. Yang, "Image reconstruction by nonlinear landweber iteration for complicated distributions," *Meas. Sci. Technol.*, vol. 19, no. 9, Sep. 2008, Art. no. 094014.

[19] J. H. Kim, "Novel iterative image reconstruction algorithm for electrical capacitance tomography: Directional algebraic reconstruction technique," *IEICE Trans. Fundam. Electron., Commun. Comput. Sci.*, vol. E89–A, no. 6, pp. 1578–1584, Jun. 2006.

[20] Q. Marashdeh, W. Warsito, L.-S. Fan, and F. L. Teixeira, "Nonlinear forward problem solution for electrical capacitance tomography using feed-forward neural network," *IEEE Sensors J.*, vol. 6, no. 2, pp. 441–449, Apr. 2006. [Online]. Available: http://ieeexplore.ieee.org/xpls/abs_all.jsp?arnumber=1608088

[21] D. Boublil, M. Elad, J. Shtok, and M. Zibulevsky, "Spatially-adaptive reconstruction in computed tomography using neural networks," *IEEE Trans. Med. Imag.*, vol. 34, no. 7, pp. 1474–1485, Jul. 2015.

[22] H. Garbaa, L. Jackowska-Strumiáo, K. Grudzieâ, and A. Romanowski, "Application of electrical capacitance tomography and artificial neural networks to rapid estimation of cylindrical shape parameters of industrial flow structure," *Arch. Electr. Eng.*, vol. 65, no. 4, pp. 657–669, Dec. 2016.

[23] W. Deabes, A. Sheta, K. E. Bouazza, and M. Abdelrahman, "Application of electrical capacitance tomography for imaging conductive materials in industrial processes," *J. Sensors*, vol. 2019, pp. 1–22, Dec. 2019.

[24] J. Li, X. Yang, Y. Wang, and R. Pan, "An image reconstruction algorithm based on RBF neural network for electrical capacitance tomography," in *6th Int. Conf. Electromagn. Field Problems Appl.*, Jun. 2012, pp. 1–4. [Online]. Available: http://ieeexplore.ieee.org/document/6310416/

[25] P. Fiderek, J. Kucharski, and R. Wajman, "Fuzzy inference for two-phase gas-liquid flow type evaluation based on raw 3D ECT measurement data," *Flow Meas. Instrum.*, vol. 54, pp. 88–96, Apr. 2017, doi: 10.1016/j.flowmeasinst.2016.12.010.

[26] W. A. Deabes and M. A. Abdelrahman, "A nonlinear fuzzy assisted image reconstruction algorithm for electrical capacitance tomography," *ISA Trans.*, vol. 49, no. 1, pp. 10–18, Jan. 2010.

[27] J. Ye, H. Wang, and W. Yang, "Image reconstruction for electrical capacitance tomography based on sparse representation," *IEEE Trans. Instrum. Meas.*, vol. 64, no. 1, pp. 89–102, Jan. 2015.

[28] L. Zhang, Y. Zhai, X. Wang, and P. Tian, "Reconstruction method of electrical capacitance tomography based on wavelet fusion," *Measurement*, vol. 126, pp. 223–230, Oct. 2018, doi: 10.1016/j.measurement.2018.05.006.

[29] C. Tan, S. Lv, F. Dong, and M. Takei, "Image reconstruction based on convolutional neural network for electrical resistance tomography," *IEEE Sensors J.*, vol. 19, no. 1, pp. 196–204, Jan. 2019. [Online]. Available: https://ieeexplore.ieee.org/document/8493596/

[30] J. Zheng and L. Peng, "An autoencoder-based image reconstruction for electrical capacitance tomography," *IEEE Sensors J.*, vol. 18, no. 13, pp. 5464–5474, Jul. 2018.

[31] J. Lei, Q. Liu, and X. Wang, "Deep learning-based inversion method for imaging problems in electrical capacitance tomography," *IEEE Trans. Instrum. Meas.*, vol. 67, no. 9, pp. 2107–2118, Sep. 2018.

[32] S. J. Hamilton, A. Hänninen, A. Hauptmann, and V. Kolehmainen, "Beltrami-net: Domain-independent deep D-bar learning for absolute imaging with electrical impedance tomography (a-EIT)," *Physiol. Meas.*, vol. 40, no. 7, Jul. 2019, Art. no. 074002.

[33] J. Xiao, Z. Liu, P. Zhao, Y. Li, and J. Huo, "Deep learning image reconstruction simulation for electromagnetic tomography," *IEEE Sensors J.*, vol. 18, no. 8, pp. 3290–3298, Apr. 2018.

[34] H. Sak, A. Senior, and F. Beaufays, "Long short-term memory recurrent neural network architectures for large scale acoustic modeling," in *15th Annu. Conf. Int. speech Commun. Assoc.*, 2014, pp. 1–8.

[35] R. Guo, J. Zhang, D. Liu, Y. Zhang, and D. Zhang, "Application of bi-directional long short-term memory recurrent neural network for seismic impedance inversion," in *Proc. 81st EAGE Conf. Exhib.*, 2019, pp. 1–5.

[36] A. Fedeli, "Microwave tomography with LSTM-based processing of the scattered field," *IEEE Open J. Antennas Propag.*, vol. 2, pp. 213–223, 2021.

[37] N. T. Nguyen, D. Q. Tran, N. T. Nguyen, and H. Q. Nguyen, "A CNN-LSTM architecture for detection of intracranial hemorrhage on CT scans," *Med. Imag. Deep Learn.*, vol. 4, pp. 1–4, Dec. 2020. [Online]. Available: https://openreview.net/forum?id=Kllq2kzsNC

[38] H. Wu, X. Ma, C.-H.-H. Yang, and S. Liu, "Attention based bidirectional convolutional LSTM for high-resolution radio tomographic imaging," *IEEE Trans. Circuits Syst. II, Exp. Briefs*, vol. 68, no. 4, pp. 1482–1486, Apr. 2021.

[39] M. H. Memon, N. A. Golilarz, J. Li, M. Yazdi, and A. Addeh, "Early detection of COVID-19 disease using computed tomography images and optimized CNN-LSTM," in *Proc. 17th Int. Comput. Conf. Wavelet Act. Media Technol. Inf. Process. (ICCWAMTIP)*, 2020, pp. 161–165.

[40] F. Demir, "DeepCoroNet: A deep LSTM approach for automated detection of COVID-19 cases from chest X-ray images," *Appl. Soft Comput.*, vol. 103, May 2021, Art. no. 107160.

[41] D. Caulk, "Analysis of mold filling in lost foam casting of aluminum: Part II-example applications," *Int. J. Metalcasting*, vol. 3, no. 1, pp. 7–25, Jan. 2009. [Online]. Available: http://link.springer.com/10.1007/BF03355438

[42] P. Foam. *Plymouth Foam*. Accessed: May 20, 2021. [Online]. Available: https://www.plymouthfoam.com/lost-foam-is-found/04colorado-04carengines-carengines/

[43] W. A. Deabes, H. H. Amin, and M. Abdelrahman, "Optimized fuzzy image reconstruction algorithm for ECT systems," in *Proc. IEEE Int. Conf. Fuzzy Syst. (FUZZ-IEEE)*, Jul. 2016, pp. 1209–1215.

[44] A. R. Smith, M. A. Abdelrahman, and W. A. Deabes, "A confidence prediction system for metal fill visualization using electrical capacitance tomography," in *Proc. 41st Southeastern Symp. Syst. Theory*, Mar. 2009, pp. 122–126.

[45] J. K. Kim, J. A. Fessler, and Z. Zhang, "Forward-projection architecture for fast iterative image reconstruction in X-ray CT," *IEEE Trans. Signal Process.*, vol. 60, no. 10, pp. 5508–5518, Oct. 2012. [Online]. Available: http://www.pubmedcentral.nih.gov/articlerender.fcgi?artid=3473087&tool=pmcentrez&rendertype=abstract

[46] M. Wang, *Industrial Tomography*. Amsterdam, The Netherlands: Elsevier, 2015. [Online]. Available: https://linkinghub.elsevier.com/retrieve/pii/C20130164665

[47] W. A. Deabes and M. Abdelrahman, "Shape reconstruction method for imaging conductive materials in electrical capacitance tomography," in *Proc. 42nd Annu. Conf. IEEE Ind. Electron. Soc.*, Oct. 2016, pp. 1055–1060. [Online]. Available: http://ieeexplore.ieee.org/document/7793270/

[48] K. H.-Y. Wei, C.-H. Qiu, and K. Primrose, "Super-sensing technology: Industrial applications and future challenges of electrical tomography," *Phil. Trans. Roy. Soc. A, Math., Phys. Eng. Sci.*, vol. 374, Jun. 2016, Art. no. 20150328. [Online]. Available: https://royalsocietypublishing.org/doi/10.1098/rsta.2015.0328

[49] I. Saied and M. Meribout, "Electronic hardware design of electrical capacitance tomography systems," *Phil. Trans. Roy. Soc. A, Math., Phys. Eng. Sci.*, vol. 374, no. 2070, pp. 03–31, Jun. 2016. [Online]. Available: http://rsta.royalsocietypublishing.org/lookup/doi/10.1098/rsta.2015.0331

[50] W. Deabes, M. Abdelrahman, and P. K. Rajan, "A new wide frequency band capacitance transducer with application to measuring metal fill time," *Sensors Transducers*, vol. 100, pp. 72–84, Jan. 2009. [Online]. Available: https://www.highbeam.com/doc/1P3-1784969121.html

[51] W. A. Deabes, M. A. Abdelrahman, and C. Murray, "Analysis, design and application of a capacitance measurement circuit with wide operating frequency range," in *Proc. IEEE Int. Conf. Control Appl.*, Dec. 2008, pp. 114–119. [Online]. Available: http://ieeexplore.ieee.org/articleDetails.jsp?arnumber=4629613

[52] W. Deabes, M. Abdelraliman, C. Murray, P. Rajan, and J. Russell, "A wide frequency range circuit for measuring mutual capacitance with application to monitoring of metal fill profile," in *Proc. Conf. Southeast-con*, Dec. 2008, pp. 362–367.

[53] W. N. Abd Rashid, E. J. Mohamad, R. Abdul Rahim, J. Abdullah, and H. L. Mohmad Ameran, "Electrical capacitance tomography: A review on portable ECT system and hardware design," *Sensor Rev.*, vol. 36, no. 1, pp. 64–70, Jan. 2016. [Online]. Available: http://www.emeraldinsight.com/doi/10.1108/SR-06-2015-0089

[54] Ø. Isaksen, "A review of reconstruction techniques for capacitance tomography," *Meas. Sci. Technol.*, vol. 7, no. 3, pp. 325–337, 1996. [Online]. Available: http://stacks.iop.org/0957-0233/7/i=3/a=013?

[55] J. Lei, S. Liu, Z. H. Li, and M. Sun, "Image reconstruction algorithm based on the extended regularised total least squares method for electrical capacitance tomography," *IET Sci., Meas. Technol.*, vol. 2, no. 5, pp. 326–336, Sep. 2008.

[56] Y. LeCun, Y. Bengio, and G. Hinton, "Deep learning," *Nature*, vol. 521, no. 7553, p. 436, 2015.

[57] D. Shen, G. Wu, and H. Suk, "Deep learning in medical image analysis," *Annu. Rev. Biomed. Eng.*, vol. 19, pp. 221–248, Jun. 2017.

[58] M. Längkvist, L. Karlsson, and A. Loutfi, "A review of unsupervised feature learning and deep learning for time-series modeling," *Pattern Recognit. Lett.*, vol. 42, pp. 11–24, Jun. 2014.

[59] G. Litjens T. Kooi, B. E. Bejnordi, A. A. A. Setio, F. Ciompi, A. Ghafoorian, J. A. W. M. van der Laak, B. van Ginneken, and C. I. Sánchez, "A survey on deep learning in medical image analysis," *Med. Image Anal.*, vol. 42, pp. 60–88, Dec. 2017.

[60] A. Kamilaris and F. X. Prenafeta-Boldú, "Deep learning in agriculture: A survey," *Comput. Electron. Agricult.*, vol. 147, pp. 70–90, Apr. 2018.

[61] J. B. Heaton, N. G. Polson, and J. H. Witte, "Deep learning for finance: Deep portfolios," *Appl. Stochastic Models Bus. Ind.*, vol. 33, no. 1, pp. 3–12, Jan. 2017.

[62] Y. Lu, "Industry 4.0: A survey on technologies, applications and open research issues," *J. Ind. Inf. Integr.*, vol. 6, pp. 1–10, Jun. 2017.

[63] R. Alkhaddar, T. Wooder, B. Sertyesilisik, and A. Tunstall, "Deep learning approach's effectiveness on sustainability improvement in the UK construction industry," *Manage. Environ. Qual., Int. J.*, vol. 23, no. 2, pp. 126–139, Feb. 2012.

[64] S. Hochreiter and J. Schmidhuber, "Long short-term memory," *Neural Comput.*, vol. 9, no. 8, pp. 1735–1780, 1997.

[65] W. Rawat and Z. Wang, "Deep convolutional neural networks for image classification: A comprehensive review," *Neural Comput.*, vol. 29, no. 9, pp. 2352–2449, Sep. 2017.

[66] A. Krizhevsky, I. Sutskever, and G. E. Hinton, "Imagenet classification with deep convolutional neural networks," in *Proc. Adv. Neural Inf. Process. Syst.*, 2012, pp. 1097–1105.

[67] D. Caulk, "A pattern decomposition model for lost foam casting of aluminum: Part II—Gap mode," *Trans. Amer. Foundry Soc.*, vol. 114, pp. 857–873, 2006. [Online]. Available: https://www.tib.eu/en/search/id/tema%3ATEMA20061005095/A-pattern-decomposition-model-for-lost-foam-casting/#documentinfo

[68] D. A. Caulk, "A pattern decomposition model for lost foam casting of aluminum: Part III—Collapse mode," *AFS Trans.*, vol. 114, pp. 1–11, Oct. 2007.

[69] W. D. Griffiths and M. J. Ainsworth, "Instability of the liquid metal–pattern interface in the lost foam casting of aluminum alloys," *Metall. Mater. Trans. A*, vol. 47, no. 6, pp. 3137–3149, Jun. 2016.

WAEL DEABES (Member, IEEE) received the B.S. and M.S. degrees in computer and electrical engineering from Mansoura University, Mansoura, Egypt, in 1999 and 2003, respectively, and the Ph.D. degree in computer engineering from Tennessee Technological University, USA, in 2010. He is currently working as an Associate Professor with the Department of Computer Science, Umm Al-Qura University, Saudi Arabia. He served as a principal investigator and a co-principal investigator for several funded grants from the King Abdulaziz City for Science and Technology and other international fund agencies. He has published one book, more than 40 articles in international journals, and more than 40 papers in international conferences, and holds one patent. His research interests include electrical tomography, artificial intelligence, control systems, the Internet of Things (IoT), smart cities, and embedded systems. He served as a Reviewer for several journals and conferences, including *ISA Transactions*, IEEE Sensors Journal, and IEEE Transactions on Image Processing.

ALAA SHETA (Member, IEEE) received the B.E. and M.Sc. degrees in electronics and communication engineering from the Faculty of Engineering, Cairo University, in 1988 and 1994, respectively, and the Ph.D. degree from the Department of Computer Science, School of Information Technology and Engineering, George Mason University, Fairfax, VA, USA, in 1997. He is currently an Associate Professor of computer science with Southern Connecticut State University. He has 22 years of experience in the area of meta-heuristics search algorithms, swarm intelligence, evolutionary computation, deep learning, modeling and simulation of dynamical nonlinear systems, image processing, optimization, fuzzy logic, and neural networks. He supervised more than 30 M.S. and Ph.D. dissertations. His research records include more than 150 conference and journal publications, six book chapters, and three books. He is also an Associate Editor of the *International Journal of Advanced Computer Science and Applications (IJACSA)*, the *International Journal of Computational Complexity and Intelligent Algorithms*, and the *International Journal of Computer Information Systems and Industrial Management Applications*.

MALIK BRAIK (Member, IEEE) received the B.Sc. degree in electrical engineering from the Faculty of Engineering, Jordan University of Science and Technology, Jordan, in 2000, the M.Sc. degree in computer science from the Department of Information Technology, Al-Balqa Applied University, Al-Salt, Jordan, in 2005, and the Ph.D. degree in computer engineering from the University of Birmingham, U.K., in 2014. He is currently working with the Department of Computer Science, Prince Abdullah Bin Ghazi Faculty of Communications and Information Technology, Al-Balqa Applied University. He has more than 50 publications. His research interests include meta-heuristics search algorithms, evolutionary computation, computer vision, pattern recognition, control, and system identification, computational intelligence, and image processing.

• • •